Eur. J. Mineral.
2018, **30**, 559–567
Published online 27 November 2017

First natural hexaferrite with mixed β″-ferrite (β-alumina) and magnetoplumbite structure from Jabel Harmun, Palestinian Autonomy

Evgeny V. GALUSKIN[1,*], Irina O. GALUSKINA[1], Remo WIDMER[2] and Thomas ARMBRUSTER[2]

[1] Faculty of Earth Sciences, Department of Geochemistry, Mineralogy and Petrography, University of Silesia, Będzinska 60, 41-200 Sosnowiec, Poland
*Corresponding author, e-mail: evgeny.galuskin@us.edu.pl
[2] Mineralogical Crystallography, Institute of Geological Sciences, University of Bern, Baltzerstr. 1+3, 3012 Bern, Switzerland

Abstract: Ferrites of K and Ba close in composition to the known synthetic compounds $KFe^{2+}_2Fe^{3+}_{15}O_{25}$ and $BaMg_2Fe^{3+}_{16}O_{27}$ were found in a thin vein, filled with magnesioferrite and khesinite, in pyrometamorphic flamite–gehlenite hornfels of the Hatrurim Complex, Palestinian Autonomy. Both ferrites are characterized by a modular structure composed of 5-layered spinel (*S*) blocks interstratified with *R*-blocks. The *R*-modules of K-ferrite are of the β-alumina type whereas those in Ba-ferrite are of the magnetoplumbite type. Rare grains of K-Ba-ferrite of intermediate composition with the empirical crystal chemical formula (EPMA): $(K_{0.57}Ba_{0.38}Na_{0.05})_{\Sigma1}(Fe^{3+}_{14.08}Mg_{1.42}Al_{0.80}Zn_{0.59}Ni_{0.16}Ca_{0.14}Cu_{0.09}Mn_{0.03}Ti_{0.03}Si_{0.02})_{\Sigma17.36}O_{25.54}$, were also discovered. The structure of the natural mixed potassium-barium ferrite was investigated by single-crystal X-ray diffraction. The hexagonal space-group symmetry ($P\bar{6}m2$, $Z=2$) with $a=5.9137(2)$ and $c=33.1450(15)$ Å is different to that ($P6_3/mmc$) of the end-members and yields alternate stacking of β-alumina type $KMg_2Fe_{15}O_{25}$ and magnetoplumbite type $BaMg_2Fe_{16}O_{27}$ "supermodules", each extending ½ of the unit cell along **c**. Raman spectroscopic study confirms the mixed character of K-Ba-ferrite structure. K-Ba-ferrite formed at non-equilibrium conditions and may be interpreted as an example of a nano-dissipative structure.

Key-words: magnetoplumbite; β-alumina; potassium and barium ferrite; mixed structure; Raman; pyrometamorphic rock; Hatrurim Complex.

1. Introduction

In pyrometamorphic rocks of the Hatrurim Complex numerous ferrites and related minerals are known (all iron as Fe^{3+}): magnesioferrite $MgFe_2O_4$, trevorite $NiFe_2O_4$, cuprospinel $CuFe_2O_4$, delafossite $CuFeO_2$, harmunite $CaFe_2O_4$, brownmillerite $Ca_2Fe(Al,Fe)O_5$, srebrodolskite $Ca_2Fe(Fe,Al)O_5$, shulamitite $Ca_3TiFe(Al,Fe)O_8$, sharyginite $Ca_3TiFe(Fe,Al)O_8$, barioferrite $BaFe_{12}O_{19}$, khesinite $Ca_4Mg_2Fe_{10}O_4[Si_2Fe_{10}O_{36}]$, dorrite $Ca_4Mg_2Fe_{10}O_4[Si_2Al_{10}O_{36}]$, and also potentially new minerals: "calcioferrite" $CaFe_{12}O_{19}$ and the *CFF*-type phases: $Ca_2Mg_2Fe_{10}(Al,Fe)_4O_{25}$ and $Ca_2Mg_2Fe_{10}(Fe,Al)_4O_{25}$ (Sharygin *et al.*, 2008, 2013; Murashko *et al.*, 2010; Galuskina *et al.*, 2014, 2017). Sharyginite is a new mineral recently discovered in an altered carbonate xenolith of the Bellerberg volcano, Eifel, Germany (Juroszek *et al.*, 2017). High-temperature oxygen-bearing minerals of the Hatrurim Complex contain mainly Fe^{3+}, which is determined by the specific oxygen-fugacity during the pyrometamorphic process. Minerals of the spinel group are an exception, as they may contain significant amounts of Fe^{2+} (Sharygin *et al.*, 2013; Galuskina *et al.*, 2014, 2017a).

Potassium contents in the above listed ferrites are close to detection limit of electron-microprobe measurements. Thus, the discovery of potentially new minerals of a series of K-, K-Ba-ferrites and associated Ba-ferrite in flamite–gehlenite hornfels of the Hatrurim Complex, Palestinian Autonomy is highly unusual. Investigation of ferrite compositions showed that the K-ferrite with the simplified formula $K(Mg,Zn)_2Fe^{3+}_{15}O_{25}$ is an approximate analogue of the synthetic phase $KFe^{2+}_2Fe^{3+}_{15}O_{25}$ (β″-ferrite, Matsui *et al.*, 1985) whereas Ba-ferrite with the simplified formula $Ba(Mg,Zn)_2Fe_{16}O_{27}$ is related in composition to the known synthetic ferrite $BaMg_2Fe^{3+}_{16}O_{27}$ (*W*-ferrite; Collomb *et al.*, 1986; Pullar, 2012). Both synthetic analogues possess modular structures composed of 5-layered spinel blocks intercalated by *R*-blocks. The *R*-block in K-ferrite (β″-ferrite) is related to the one of β-alumina (Matsui *et al.*, 1985), and in Ba-ferrite (*W*-ferrite) it resembles the one of magnetoplumbite (Collomb *et al.*, 1986).

https://doi.org/10.1127/ejm/2018/0030-2697
0935-1221/18/0030-2697 $ 4.05

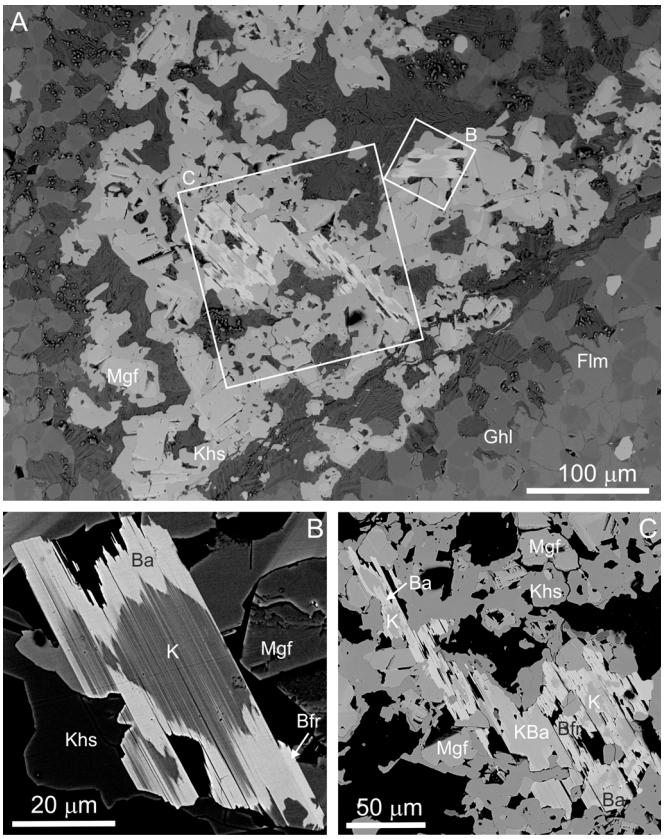

Fig. 1. (A) Ferrite veins in flamite–gehlenite hornfelse from Jabel Harmun, areas magnified in (B) and (C) are shown by frames. (B) K-ferrite phase is usually replaced by the Ba-ferrite phase and shows epitactic overgrowth by barioferrite. (C) Rare grains of K-Ba-ferrite within khesinite–magnesioferrite aggregates with K-ferrite relics replaced by Ba-ferrite with barioferrite overgrowth. Flm = flamite, Ghl = gehlenite, Mgf = magnesioferrite, Khs = khesinite, Brf = barioferrite, K = K-ferrite, Ba = Ba-ferrite, KBa = K-Ba-ferrite.

We were unable to study the crystal structures of the new natural K- and Ba-ferrites because of small sizes of their single-crystal individuals, limited amount of material, and difficulties of grain separation. Under mechanical influence the crystals fractured to extremely thin foliated fragments. Though, we were able to select a grain of K-Ba-ferrite of intermediate composition, for which structural study gave unexpected results. That crystal turned out to be the first natural ferrite with an ordered interstratification of *R*-modules of magnetoplumbite and β″-ferrite (β-alumina) types along the **c** axis. There are two known synthetic aluminates ~$Nd_{0.9}Na_{1.3}Al_{23}O_{36.5}$ ($P\bar{6}m2$, Z=1; a = 5.57 and c = 22.25 Å, Kahn & Thery, 1986) and $Sr_2MgAl_{22}O_{36}$ ($P\bar{6}m2$, Z=1; a = 5.583 and c = 22.225 Å; Iyi & Göbbels, 1996), which possess ordered mixed β-alumina and magnetoplumbite structures of similar type corresponding to natural K-Ba-ferrite.

In this paper, dedicated to the 80th birthday of Giovanni Ferraris and Stefano Merlino, we provide results of composition, structure investigation and Raman spectroscopy of this unusual K-Ba-ferrite, which has not only a modular structure composed of *R* and *S* blocks, but also represents an ordered arrangement of two different "supermodules". In addition, data on composition and Raman spectra of associated ferrites are presented.

2. Description of ferrites

Pyrometamorphic rocks of the Jabel Harmun, the Hatrurim Complex are strongly altered by secondary carbonate and calcium hydrosilicate assemblages (Galuskina *et al.*, 2014). Between the relics of pyrometamorphic rocks we distinguish mainly larnite-bearing pseudoconglomerates, a few outcrops of jasmundite–flamite rocks, and rare bodies of flamite–gehlenite hornfels. In flamite–gehlenite hornfels of the pyrometamorphic Hatrurim Complex at the Jabel Harmun locality, Palestinian Autonomy, Israel, a fine vein less than 1 mm in thickness filled with magnesioferrite and khesinite was detected. Inside this vein, K- and Ba-ferrites were sporadically observed (Fig. 1A). Jabel Harmun is the type locality for several high-temperature minerals: harmunite, $CaFe_2O_4$ (Galuskina *et al.*, 2014), vapnikite, Ca_3UO_6 (Galuskin *et al.*, 2014), nabimusaite, $KCa_{12}(SiO_4)_2(SO_4)_2O_2F$ (Galuskin *et al.*, 2015a), dzierżanowskite, $CaCu_2S_2$ (Galuskina *et al.*, 2017b), and fluormayenite, $Ca_{12}Al_{14}O_{32}F_2$ (Galuskin *et al.*, 2015b). The geological setting and also the main hypotheses of formation of the rocks at the Hatrurim Complex and the Jabel Harmun location were presented by Kolodny & Gross (1974), Novikov *et al.* (2013) and Galuskina *et al.* (2014).

Table 1. Chemical composition of ferrites from flamite–gehlenite hornfels, Jabel Harmun, Palestinian Autonomy, wt%.

	1			2			3			4			5			6
	Mean 7	s.d.	Range	Mean 15	s.d.	Range	Mean 13	s.d.	Range	Mean 9	s.d.	Range	Mean 5	s.d.	Range	Mean 2
Na_2O	n.d.	–	–	n.d.			0.03	0.02	0.05–0.13	0.10	0.03	0.02–0.07	0.11	0.01	0.10–0.13	0.06
MgO	8.81	0.44	8.20–9.59	1.51	0.14	1.24–1.71	3.69	0.26	2.84–3.96	2.87	0.33	2.38–3.31	4.04	0.25	3.82–4.39	0.39
Al_2O_3	2.67	0.14	2.46–2.89	7.94	0.37	7.41–8.69	3.01	0.10	2.88–3.20	2.31	0.06	2.24–2.42	2.87	0.08	2.77–2.97	2.11
SiO_2	n.d.	–	–	5.09	0.54	4.17–5.73	0.08	0.03	0.03–0.13	0.05	0.02	0–0.08	0.09	0.01	0.08–0.10	n.d.
CaO	0.72	0.25	0.48–1.22	14.21	0.33	13.74–14.66	0.68	0.10	0.49–0.87	0.76	0.07	0.68–0.90	0.56	0.03	0.52–0.60	0.97
K_2O	n.d.	–	–	n.d.	–	–	2.84	0.21	2.38–3.18	0.07	0.02	0.04–0.12	1.88	0.12	1.79–2.04	0.06
TiO_2	n.d.	–	–	0.65	0.04	0.57–0.70	0.20	0.03	0.15–0.25	0.58	0.20	0.23–0.80	0.14	0.03	0.11–0.18	1.78
Cr_2O_3	0.16	0.04	0.11–0.22	0.73	0.38	0.16–1.29	0.13	0.05	0.06–0.21	n.d.	–	–	n.d.	–	–	n.d.
Fe_2O_3	68.14	0.47	75.97–77.17	68.55	1.29	66.84–70.77	80.65	0.41	79.97–81.66	80.07	0.50	79.06–80.51	79.21	0.51	78.82–79.93	80.80
MnO	0.15	0.02	0.11–0.17	n.d.	–	–	0.12	0.04	0.07–0.21	0.15	0.04	0.09–0.22	0.15	0.01	0.14–0.16	n.d.
SrO	n.d.	–	–	n.d.	–	–	n.d.	–	–	n.d.	–	–	n.d.	–	–	n.d.
BaO	n.d.	–	–	n.d.	–	–	1.81	0.50	1.05–2.90	8.24	0.53	7.52–9.04	4.15	0.43	3.80–4.75	11.43
NiO	2.08	0.15	1.75–2.25	n.d.	–	–	0.75	0.07	0.55–0.83	0.78	0.07	0.68–0.88	0.83	0.06	0.76–0.91	n.d.
CuO	1.15	0.18	0.94–1.45	n.d.	–	–	0.54	0.07	0.44–0.63	0.45	0.04	0.38–0.53	0.52	0.08	0.41–0.60	n.d.
ZnO	5.83	0.30	5.35–6.19	0.20	0.10	0.02–0.36	3.09	0.22	2.49–3.48	2.15	0.17	1.87–2.36	3.28	0.20	3.00–3.42	0.53
FeO	7.54	–	–	–	–	–	–	–	–	–	–	–	–	–	–	–
Total	97.25	–	–	98.88	–	–	97.62	–	–	98.58	–	–	97.83	–	–	98.12
Ba	–	–	–		–	–	0.16	–	–	0.82	–	–	0.38	–	–	0.82
K	–	–	–		–	–	0.83	–	–	0.02	–	–	0.57	–	–	0.01
Na	–	–	–		–	–	0.01	–	–	0.05	–	–	0.05	–	–	0.02
Ca	0.03	–	–	5.03	–	–	0.17	–	–	0.21	–	–	0.14	–	–	0.19
Mn^{2+}	0.01	–	–		–	–	0.02	–	–	0.03	–	–	0.03	–	–	–
Mg	0.48	–	–	0.74	–	–	1.26	–	–	1.09	–	–	1.42	–	–	0.11
Ni	0.06	–	–		–	–	0.14	–	–	0.16	–	–	0.16	–	–	–
Cu	0.03	–	–		–	–	0.09	–	–	0.09	–	–	0.09	–	–	–
Zn	0.16	–	–	0.05	–	–	0.54	–	–	0.41	–	–	0.59	–	–	0.07
Fe^{2+}	0.23	–	–		–	–		–	–		–	–		–	–	–
Al	0.12	–	–	3.09	–	–	0.81	–	–	0.69	–	–	0.80	–	–	0.45
Cr^{3+}	0.01	–	–	0.19	–	–	0.02	–	–		–	–		–	–	–
Fe^{3+}	1.88	–	–	17.04	–	–	13.90	–	–	15.26	–	–	14.08	–	–	11.08
Si	–	–	–	1.68	–	–	0.02	–	–	0.01	–	–	0.02	–	–	–
Ti^{4+}	–	–	–	0.16	–	–	0.03	–	–	0.11	–	–	0.03	–	–	0.24

1 – magnesioferrite, formula calculated on 8 O; 2 – khesinite, formula calculated on 80 O; 3 – K-ferrite, formula calculated on 25 O, 4 – Ba-ferrite, formula calculated on 27 O; 5 – K-Ba-ferrite, formula calculated on cations and normalised on 1 (Ba+K+Na) pfu; 6 – barioferrite, formula calculated on 19 O.

Chemical compositions of ferrites were examined using the CAMECA SX100 electron microprobe (Institute of Geochemistry, Mineralogy and Petrology, University of Warsaw) at 15 kV, 20 nA and 1–3 μm beam diameter using the following lines and standards: Ca*K*α, Si*K*α = wollastonite; Al*K*α, K*K*α = orthoclase; Cr*K*α = Cr_2O_3; Fe*K*α = hematite; Mn*K*α = rhodochrosite; Ti*K*α = rutile; Mg*K*α = diopside; Na*K*α = albite; Ba*L*α = baryte; Sr*L*α = $SrTiO_3$, Cu*K*α = Cu_2O; Ni*K*α = NiO and Zn*K*α = sphalerite.

Both magnesioferrite and khesinite are compositionally slightly different to the corresponding minerals of the khesinite holotype material (Table 1, Galuskina *et al.*, 2017a). Magnesioferrite, $(Mg_{0.48}Fe^{2+}_{0.23}Zn_{0.17}Ni_{0.06}Cu_{0.03}Ca_{0.03})_{\Sigma1}(Fe^{3+}_{1.88}Al_{0.12})_{\Sigma2}O_4$, contains increased Fe^{2+} and Zn contents, whereas khesinite, $Ca_4(Ca_{1.03}Mg_{0.74}Zn_{0.05}Fe^{3+}_{1.88})_{\Sigma2}(Fe^{3+}_{9.4}Cr^{3+}_{9.64}Ti_{0.17})_{\Sigma10}(Fe^{3+}_{7.23}Al_{3.09}Si_{1.68})_{\Sigma12}O_{40}$, has higher Ca content.

The K-ferrite crystallized in cavities of khesinite–magnesioferrite aggregates, later it was replaced by Ba-ferrite (Fig. 1A and B). The mean composition of K-ferrite (Table 1) corresponds to the crystal-chemical formula: $(K_{0.83}Ba_{0.16}Na_{0.01})_{\Sigma1}(Fe^{3+}_{13.90}Mg_{1.26}Al_{0.81}Zn_{0.54}Ti_{0.03}Ca_{0.17}Ni_{0.14}Cu_{0.09}Cr^{3+}_{0.02}Mn_{0.02}Si_{0.02})_{\Sigma17}O_{25}$. The simplified formula of K-ferrite can be represented as (K,Ba)(Mg,Zn,Ca,Ni,Cu)$_2$(Fe^{3+},Al)$_{15}O_{25}$, that leads to the ideal formula $KMg_2Fe_{15}O_{25}$, *i.e.*, this phase can be tentatively considered as Mg-analogue of the synthetic phase $KFe^{2+}_2Fe^{3+}_{15}O_{25}$ (β″-ferrite, Matsui *et al.*, 1985).

The Ba-ferrite has the mean composition corresponding to the empirical formula $(Ba_{0.82}Ca_{0.11}Na_{0.05}K_{0.02})_{\Sigma1}(Fe^{3+}_{15.26}Mg_{1.09}Al_{0.69}Zn_{0.41}Ti_{0.11}Ca_{0.09}Ni_{0.16}Cu_{0.09}Mn_{0.03}Si_{0.01})_{\Sigma17.94}O_{27}$ (Table 1), forming reaction rims on K-ferrite (Fig. 1B). The empirical formula may be simplified to (Ba,Ca)(Mg,Zn,Ni,Ca,Cu)$_2$(Fe^{3+},Al,Ti)$_{16}O_{27}$. Thus, it is a natural analogue of the known synthetic phase $BaMg_2Fe^{3+}_{16}O_{27}$ (*W*-ferrite, Collomb *et al.*, 1986; Pullar, 2012).

Barioferrite, $(Ba_{0.82}Ca_{0.15}Na_{0.02}K_{0.01})_{\Sigma1}(Fe^{3+}_{11.09}Al_{0.45}Ti_{0.24}Mg_{0.11}Zn_{0.07}Ca_{0.04})_{\Sigma12}O_{19}$, is the latest ferrite in the vein. It commonly forms epitactic overgrowth on Ba-ferrite (Fig. 1B). The composition of barioferrite is close to the well-studied synthetic phase $BaFe_{12}O_{19}$ (*M*-ferrite) and has a structure with only 3-layered spinel blocks intercalated by *R*-blocks of the magnetoplumbite type (Townes *et al.*, 1967; Pullar, 2012). Thus, barioferrite (*M*-ferrite) and Ba-ferrite (*W*-ferrite) are different polysomes distinguished by the number of spinel layers in the *S* block (3 *versus* 5).

In backscattered electron (BSE) images there is an additional homogeneous grey phase, darker than Ba-ferrite but lighter than K-ferrite (Fig. 1C). This phase shows intermediate composition between the end-members K- and Ba-ferrite: $(K_{0.57}Ba_{0.38}Na_{0.05})_{\Sigma1}(Fe^{3+}_{14.08}Mg_{1.42}Al_{0.80}Zn_{0.59}Ni_{0.16}Ca_{0.14}Cu_{0.09}Mn_{0.03}Ti_{0.03}Si_{0.02})\Sigma_{17.36}O_{25.54}$ (Table 1). A grain of that phase, 50 × 50 × 10 μm in size, was extracted for single-crystal X-ray diffraction investigation.

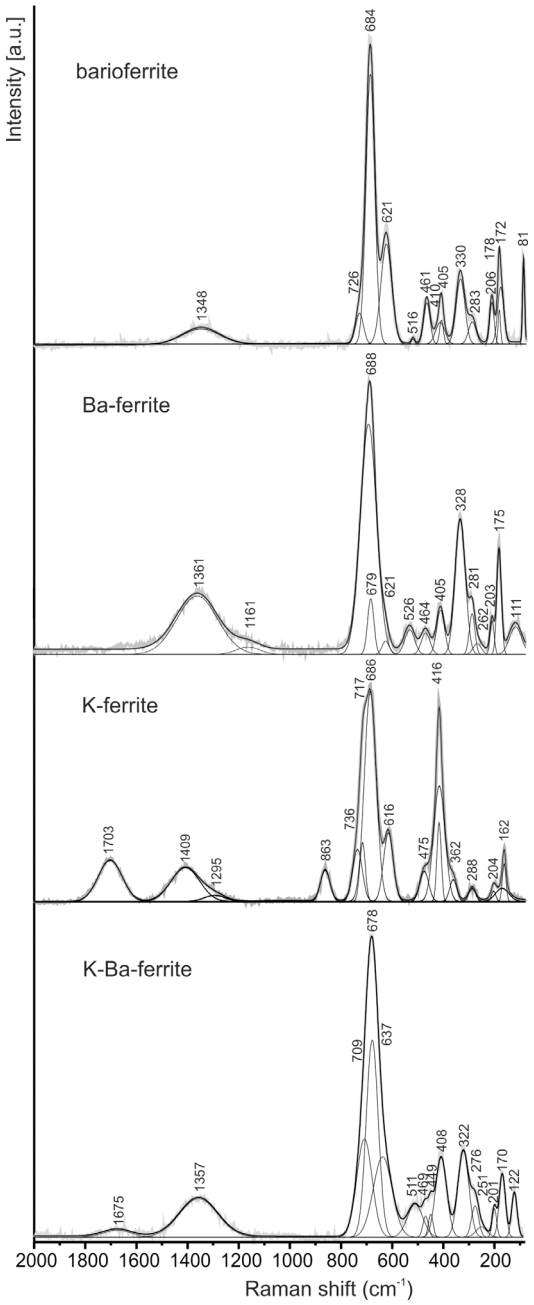

Fig. 2. Raman spectra of ferrites from Jabel Harmun.

3. Raman spectroscopy of ferrites

Raman spectra of K-ferrite, Ba-ferrite, K-Ba-ferrite and barioferrite (Fig. 2) were recorded on a WITec alpha 300R Confocal Raman Microscope (Department of Earth Science, University of Silesia, Poland) equipped with an air-cooled solid laser (532 nm) and a CCD camera operating at −61 °C. An air Zeiss LD EC Epiplan-Neofluan DIC – 100/0.75NA objective was used. Raman scattered light was focused through a broad-band single-mode fibre with effective pinhole size of about 30 μm and a monochromator with 600 mm^{-1} grating. The power of the laser at the sample position was ~40 mW. Integration

times of 5 s with accumulation of 15 scans and a resolution 3 cm^{-1} were chosen. The monochromator was calibrated using the Raman scattering line of a silicon plate (520.7 cm^{-1}).

The Raman spectrum of barioferrite corresponds to the spectrum of synthetic $BaFe_{12}O_{19}$. The interpretation of strong bands, related mainly to vibrations of Fe–O in different polyhedra (cm^{-1}), is as follows: 719 (synthetic analogue)/726 (our data) (A_{g1}) FeO_4-tetrahedra, spinel(*S*)-block; 684/684 (A_{g1}) FeO_5-bipyramid, *R*-block; 614/621 (A_{g1}) FeO_6-octahedra, *R*-block; 467/461 (A_{g1}) FeO_6-octahedra, *S*-block; 409/405 (A_{g1}) FeO_6-octahedra, *S*-block; 335/330 (A_{g1}) FeO_6-octahedra mixed; 173/172 (E_{1g}) whole spinel block (Fig. 2, Kreisel *et al.*, 1998; Silva Júnior and Paschoal, 2014). Besides, a strong band at 81 cm^{-1} in the barioferrite spectrum is assigned to Ba-related vibrations. Overtones above 1300 cm^{-1} are also noted (Fig. 2).

Raman spectra of Ba-ferrite and K-Ba-ferrite resemble the barioferrite spectrum. The strongest band in the barioferrite spectrum at 684 cm^{-1} is attributed to vibrations of Fe–O in the FeO_5-bipyramid, which belongs to the *R*-block of the magnetoplumbite type (Kreisel *et al.*, 1998). Bands at 688 cm^{-1} and 678 cm^{-1} agree with those bands in spectra of Ba-ferrite and K-Ba-ferrite, respectively (Fig. 2). The band at 621 cm^{-1}, well expressed in the barioferrite spectrum is related to vibrations in FeO_6-octahedra belonging to magnetoplumbite *R*-block (Kreisel *et al.*, 1998). However, this band is week in the spectra of Ba- and K-Ba-ferrites (Fig. 2). In Ba-ferrite a strong band at 328 cm^{-1} can be interpreted as originated from bending vibrations in FeO_6-octahedra belonging to the magnetoplumbite *R*-block (Fig. 2).

The band at 686cm^{-1} in the K-ferrite spectrum, also observed in other studied ferrites, is the strongest (Fig. 2). Additional strong bands at 736, 717 cm^{-1}, and 416 cm^{-1} are related to stretching and bending vibrations of FeO_4-terahedra in the *R*-blocks of the β-alumina type.

In K-Ba-ferrite additional bands at 408 and 322 cm^{-1} (bending vibrations) are of similar intensity (Fig. 2) and may represent characteristic signs for the presence of different *R*-blocks: β-alumina and magnetoplumbite.

The origin of the strong bands at 686 and 616 cm^{-1} in the K-ferrite spectrum (Fig. 2) is still open, FeO_5-bipyramids and FeO_6-octahedra in *R*-blocks do not exist in the K-ferrite structure (Matsui *et al.*, 1985). It seems that these bands in K-ferrite and probably in other Ba- and K-Ba-ferrites as well are of complex nature and may be related to stretching vibrations in FeO_4-tetrahedra and FeO_6-octahedra in the spinel blocks.

4. Structure of K-Ba-ferrite

4.1. Experimental procedure

X-ray diffraction data for a single crystal of K-Ba-ferrite were collected using a Bruker SMART APEX II CCD diffractometer installed at University of Bern. Intensity data were measured at room temperature using graphite-monochromatized Mo*K*α radiation (λ = 0.71069 Å). Preliminary lattice parameters and an orientation matrix were obtained from three sets of frames and refined during the integration process of the intensity data. Diffraction data were collected with ω scans at different ϕ settings (ϕ-ω scan) (Bruker, 1999). Data were processed using SAINT (Bruker, 1999). An empirical absorption correction using SADABS (Sheldrick, 1996) was applied. The structure was solved by direct methods using SHELXS and refinements were done using SHELXL (Sheldrick, 2008). Scattering factors for neutral atoms were used throughout. The intensity data set of 13885 reflections revealed $P6_3/mmc$ pseudo-symmetry as known as correct symmetry for $BaMg_2Fe_{16}O_{27}$, $Z = 2$, $a = 5.9060(7)$ and $c = 32.915(7)$ Å (Collomb *et al.*, 1986). However, in the data set of natural K-Ba-ferrite there were also 247 weak but significant reflections violating screw axes (*e.g.* 6_3) and glide planes. Thus, the true symmetry of the investigated crystal must be significantly lower. Test trials in space group *P*3 indicated that the two *R*-blocks, characteristic of magnetoplumbite-group structures with *ca.* 33 Å periodicity along **c**, are not related by symmetry. In addition, mirror planes perpendicular to **c** were found through the *R*-blocks at $z = 0$ and $z = ½$. Thus, the observed 3/*m* symmetry indicated space group $P\bar{6}$ or $P\bar{6}m2$. Subsequent structure solution and refinements were done in both space groups. *P*6*m*2 required the lower number of parameters and was finally chosen. This space

Table 2. Crystal data and refinement parameters of mixed K-Ba-ferrite.

Crystal data	Crystal no. 1
a-axis (Å)	5.9137(2)
c-axis (Å)	33.1450(15)
Cell volume (Å^3)	1003.85(7)
Z	2
Space group	$P\bar{6}m2$
Refined formula	$K_{0.59}Ba_{0.41}Me_{17.38}O_{25.56}$
Intensity measurement	
Diffractometer	APEX II SMART
X-ray radiation	Mo*K*α λ = 0.71073 Å
X-ray power	50 kV, 30 mA
Monochromator	Graphite
Temperature	25°C
Time per frame	60 s
Max. θ°	30.56
Index ranges	$-8 \le h \le 8$ $-6 \le k \le 7$ $-47 \le l \le 47$
No. of measured reflections	13 885
No. of unique reflections	1340
No. of observed reflections $I>2\sigma(I)$	1090
Structure refinement	–
No. of parameters used in the refinement	90
R(int)	0.0647
R(σ)	0.0351
GooF	1.128
*R*1, $I>2\sigma(I)$	0.0606
*R*1, all data	0.0761
*wR*2 (on F^2)	0.1434
$\Delta\rho_{min}$ ($-$eÅ^{-3})	3.2
$\Delta\rho_{max}$ (eÅ^{-3})	2.8

Table 3. Atomic coordinates, $U^{iso/eq}$, and occupancies of mixed K-Ba-ferrite.

Site	Atom	*x*	*y*	*z*	$U^{iso/eq}$	Occupancy
Fe1	Fe	0	0	0.15730(13)	0.0076(7)	1
Fe2	Fe	−⅔	⅔	0.33989(13)	0.0057(7)	1
Fe3	Fe	−⅓	⅓	0.19334(13)	0.0063(7)	1
Fe4	Fe	−⅓	⅓	0.30255(12)	0.0067(7)	1
Fe5	Fe	−0.4985(3)	0.0030(7)	0.10053(6)	0.0073(4)	1
Fe6	Fe	0.1697(5)	−0.1697(5)	0.24822(8)	0.0070(6)	0.631(15)
Mg6	Mg	0.1697(5)	−0.1697(5)	0.24822(8)	0.0070(6)	0.369(15)
Fe7	Fe	0	0	0.32135(15)	0.0081(12)	0.81(3)
Mg7	Mg	0	0	0.32135(15)	0.0081(12)	0.19(3)
Fe8	Fe	−⅔	−⅓	0.17544(16)	0.0078(12)	0.81(3)
Mg8	Mg	−⅔	−⅓	0.17544(16)	0.0078(12)	0.19(3)
Fe9	Fe	−0.6613(7)	0.1693(4)	0.39621(6)	0.0091(5)	1
Fe10	Fe	0	0	0.04564(17)	0.0217(10)	1
Fe11	Fe	⅓	⅔	0	0.026(3)	0.76(3)
Fe12	Fe	−⅔	⅔	0.44613(13)	0.0130(8)	1
Ba1	Ba	−⅓	⅓	0	0.0092(11)	0.56(2)
K1	K	−⅓	⅓	0	0.0092(11)	0.44(2)
Ba2	Ba	⅔	⅓	½	0.056(4)	0.27(3)
K2	K	⅔	⅓	½	0.056(4)	0.73(3)
O1	O	0	0	0.4232(5)	0.003(3)	1
O2	O	−⅓	⅓	0.3599(6)	0.014(4)	1
O3	O	−0.1519(12)	0.1519(12)	0.2839(3)	0.006(2)	1
O4	O	−0.5034(16)	0.5034(16)	0.2130(3)	0.010(2)	1
O5	O	−0.8441(13)	0.8441(13)	0.3571(3)	0.008(2)	1
O6	O	−0.4945(18)	0.4945(18)	0.4267(3)	0.013(2)	1
O7	O	0	0	0.2117(5)	0.002(3)	1
O8	O	−⅔	⅔	0.2805(5)	0.003(3)	1
O9	O	−⅓	⅓	0.1358(5)	0.007(3)	1
O10	O	0.1771(13)	0.354(3)	0.1395(3)	0.011(2)	1
O11	O	−0.1682(13)	0.1682(13)	0.0713(2)	0.0013(16)	1
O12	O	−⅔	−⅓	0.0700(6)	0.014(4)	1
O13	O	−⅔	⅔	½	0.022(7)	1
O14	O	0.148(2)	0.852(2)	0	0.016(6)	0.71(5)

U^{iso} for metals sites refers to U^{eq}.

group was also chosen by Kahn & Thery (1986) and Iyi & Göbbels (1996) for synthetic aluminates with a "super-modular" structure related to β-alumina.

Initially all octahedrally or tetrahedrally coordinated metal sites within the *S*(spinel)-block were refined with Fe scattering factors assuming full occupancy. If the isotropic displacement parameter appeared too low, Mg and Fe were refined at those sites. Due to the similar number of electrons for Mg (12) and Al (13), Mg scattering factors were used as dummy values to represent both species. With a corresponding argument, Fe represents all first-row transition metals. According to chemical data, K and Ba were assigned to the large cation position in the *R*-block and their ratio was refined. Metal sites were refined with anisotropic displacement parameters U^{ij} whereas U^{iso} was used for O sites. Experimental data and results of the structure refinement are summarized in Tables 2–5.

4.2. Results and discussion

As consequence of the low space-group symmetry, the surprising result (Fig. 3) was that one *R*-block (at $z = 0, 1$) is mainly occupied by Ba (0.56(2) Ba + 0.44(2) K) whereas the second *R*-block (at $z = ½$) is dominated by K (0.73(3) K + 0.27(3) Ba). In the reference structure of $BaMg_2Fe_{16}O_{27}$ (Collomb *et al.*, 1986) the symmetry-equivalent magnetoplumbite-type *R*-blocks are completed by face-sharing octahedra and an additional trigonal bipyramid, which connect along **c** two adjacent sheets of octahedra. The same topological arrangement also occurred in the Ba-dominant *R*-block of natural K-Ba-ferrite (Fig. 3). In the β″-ferrite (β-alumina)-type structure of $KFe_2^{2+}Fe_{15}^{3+}O_{25}$ (Matsui *et al.*, 1986) with $a \approx 5.9$ and $c \approx 33$ Å and space group $P6_3/mmc$, the two symmetry-equivalent K-bearing *R*-blocks have additionally two corner-sharing tetrahedra, which connect along **c** two adjacent sheets of octahedra. Corresponding tetrahedra (Fe12) were also analysed in the K-dominant *R*-block of natural K-Ba-ferrite (Fig. 3). However, there is additional disorder in the Ba-rich *R*-block (at $z = 0, 1$). Due to the partial replacement of Ba by K, the oxygen atoms (O14) forming the cross-section of the trigonal bipyramid are only 0.71(5) occupied and a corresponding value of 0.76 (3) was refined for Fe11 at the centre of the bipyramid. O14 also forms the common triangular face between the face-sharing octahedra around fully occupied Fe10. If ⅔ of O14 are locally missing, Fe10 adopts distorted tetrahedral coordination. The connection of Fe10 tetrahedra via O14

Table 4. Anisotropic displacement parameters (Å^2) for mixed K-Ba-ferrite.

	U^{11}	U^{22}	U^{33}	U^{23}	U^{13}	U^{12}
Fe1	0.0026(10)	0.0026(10)	0.0178(19)	0	0	0.0013(5)
Fe2	0.0050(10)	0.0050(10)	0.0072(15)	0	0	0.0025(5)
Fe3	0.0064(11)	0.0064(11)	0.0062(15)	0	0	0.0032(6)
Fe4	0.0062(11)	0.0062(11)	0.0077(15)	0	0	0.0031(6)
Fe5	0.0025(6)	0.0024(9)	0.0169(9)	−0.0009(10)	−0.0005(5)	0.0012(5)
Fe6	0.0057(8)	0.0057(8)	0.0113(11)	−0.0015(5)	0.0015(5)	0.0041(9)
Fe7	0.0056(14)	0.0056(14)	0.013(2)	0	0	0.0028(7)
Fe8	0.0027(14)	0.0027(14)	0.018(2)	0	0	0.0014(7)
Fe9	0.0061(10)	0.0066(7)	0.0146(9)	0.0010(5)	0.0020(10)	0.0030(5)
Fe10	0.0041(11)	0.0041(11)	0.057(3)	0	0	0.0020(6)
Fe11	0.009(3)	0.009(3)	0.060(7)	0	0	0.0045(15)
Fe12	0.0111(12)	0.0111(12)	0.0169(19)	0	0	0.0055(6)
Ba1	0.0087(13)	0.0087(13)	0.0103(18)	0	0	0.0043(6)
K2	0.057(5)	0.057(5)	0.054(6)	0	0	0.029(2)

Table 5. Selected bond lengths (Å) for mixed K-Ba-ferrite.

Atom	−Atom	Distance		Atom	−Atom	Distance	
Fe1	O7	1.804(16)		Fe8	O10	1.995(13)	×3
Fe1	O10	1.908(13)	×3	Fe8	O4	2.085(15)	×3
Mean		1.882		Mean		2.040	
Fe2	O5	1.904(13)	×3	Fe9	O6	1.948(10)	×2
Fe2	O8	1.968(18)	–	Fe9	O1	1.951(8)	
Mean		1.92		Fe9	O2	2.066(12)	
Fe3	O4	1.860(16)	×3	Fe9	O5	2.114(7)	×2
Fe3	O9	1.908(18)		Mean		2.023	
Mean		1.872		Fe10	O11	1.921(13)	×3
Fe4	O2	1.90(2)		Fe10	O14	2.142(19)	×3
Fe4	O3	1.959(12)	×3	Mean		2.031	
Mean		1.944		Fe11	O14	1.90(3)	×3
Fe5	O11	1.950(7)	×2	Fe11	O12	2.32(2)	×2
Fe5	O12	1.997(10)		Mean		2.068	
Fe5	O9	2.056(11)		Fe12	O13	1.786(4)	
Fe5	O10	2.107(8)	×2	Fe12	O6	1.878(19)	×3
Mean		2.028		Mean		1.855	
Fe6	O8	1.988(11)		Ba1	O11	2.905(10)	×6
Fe6	O3	2.033(7)	×2	Ba1	O14	2.963(2)	×6
Fe6	O4	2.041(9)	×2	Mean		2.934	
Fe6	O7	2.118(10)		K2	O6	2.938(13)	×6
Mean		2.042		K2	O13	3.4143(1)	×3
Fe7	O5	1.988(12)	×3	Mean		3.097	
Fe7	O3	1.990(11)	×3				
Mean		1.989					

leads to a corresponding arrangement as seen for Fe12 in the K-dominant *R*-block ($z = ½$). In other words, the polyhedral arrangement in the average *R*-block at $z = 0$, 1 represents a mixture of Ba and K characteristic features.

The tetrahedral sites Fe1–Fe4 of the *S*-block (Fig. 3) do not indicate any substitution by light elements (Mg, Al) but their average Fe–O distances vary between 1.881 and 1.944 Å (Table 5). The octahedral sites Fe5–Fe9 of the *S*-block have average Fe–O distances between 1.989 and 2.040 Å. In the mixed spinel sheets occupied by octahedra and tetrahedra, the relatively large tetrahedra Fe2 and Fe4 ($\langle$Fe–O$\rangle$ = 1.921 and 1.944 Å, respectively) are associated with small Fe7 octahedra ($\langle$Fe–O$\rangle$ = 1.989 Å), whereas the small tetrahedra Fe1 and Fe3 (Fe–O = 1.881 and 1.872 Å, respectively) are associated with the large Fe8 octahedra (Fe–O = 2.040 Å). Light elements (Mg, Al) were determined for Fe7 (19%), Fe8 (19%), and Fe6 (37%). Their average Me–O distances of 1.989, 2.04, and 2.04 Å, respectively, are not significantly different to pure Fe octahedra in the *S*-block. Thus, one could assume that the light elements may represent a combination of both the large Mg and the small Al. In the synthetic reference structure of $BaMg_2Fe_{16}O_{27}$ (Collomb *et al.*, 1986), the highest Mg substitution (38%) was determined for the central octahedral sheet (Me–O = 2.044 Å), corresponding to Fe6 in our structure model (Fig. 3). Thus, the similarity

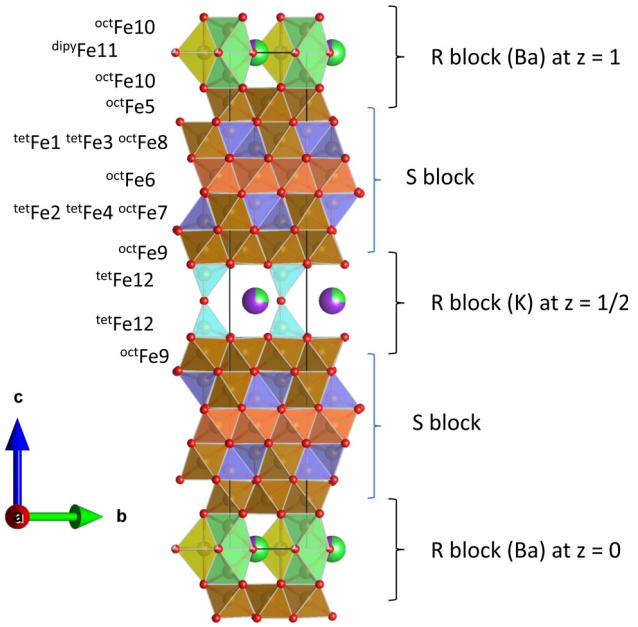

Fig. 3. Crystal structure of natural K, Ba-ferrite, space group $P\bar{6}m2$. Spinel (*S*) blocks are composed of brown octahedra (orange brown octahedra indicate increased Mg, Al content) and blue Fe tetrahedra. The *R*-block at $z = ½$ is K-rich (lilac sphere sectors). Connectivity to octahedral sheets of adjacent spinel blocks is achieved by edge-connected Fe12 tetrahedra (light blue). The *R*-block at $z = 0, 1$ is Ba-rich (green sphere sectors). Connectivity to octahedral sheets of adjacent spinel blocks is achieved by face-sharing Fe10 octahedra (green) and the Fe11 trigonal bipyramids (yellow).

in average Me–O distances and degree of substitution in both structures suggest that, at least for Fe6 in our model, mainly Mg must be assumed as light element. The Fe5 and Fe9 octahedra in the octahedral sheets adjacent to the *R*-blocks do not show light elements and have $\langle Fe–O \rangle = 2.024$ and 2.037 Å, respectively (Table 5). In contrast to our structure, $BaMg_2Fe_{16}O_{27}$ (Collomb *et al.*, 1986) shows also Mg substitution between 10 and 16% at tetrahedrally coordinated metal sites in the *S*-block.

The observation of "supermodular" order of different *R*-blocks is not unique but has been observed before for synthetic aluminates (Kahn & Thery, 1986; Iyi & Göbbels, 1996). However, both structures have only a 3-layered *S*-block in contrast to natural K-Ba-ferrite with 5-layered *S*-block. Special is the structure of $Sr_2MgAl_{22}O_{36}$ (Iyi & Göbbels, 1996), in which the same large cation (Sr) occupies alternate magnetoplumbite type and β-aluminate type *R*-blocks. Thus, this structure is assembled of ordered $SrAl_{12}O_{19}$ and $SrMgAl_{10}O_{17}$ "supermodules" (Iyi & Göbbels, 1996).

From the discussion above and the refined K/Ba ratio of 0.59/0.41 for natural K-Ba-ferrite, one could assume that by applying the reference structures the composition may be approximated by $0.59 \times KMe^{2+}_2Me^{3+}_{15}O_{25} + 0.41 \times BaMe^{2+}_2Me^{3+}_{16}O_{27} = K_{0.59}Ba_{0.41}Me^{2+}_2Me^{3+}_{15.41}O_{25.82}$. The refined composition, without distinction between Me^{3+} and Me^{2+}, is $K_{0.59}Ba_{0.41}Me_{17.38}O_{25.56}$. Assuming charge balance, the formula may be rewritten to $K_{0.59}Ba_{0.41}Me^{2+}_{2.43}Me^{3+}_{14.95}O_{25.56}$ and it is close to the mean composition measured with microprobe (Table 1). The lower O and higher Me^{2+} content of the refined formula compared to the theoretical one is mainly due to missing low-occupancy face-sharing octahedra and trigonal bipyramid in the K-dominant *R*-block (at $z = ½$), although a Ba substitution of 27% was refined. This missing Ba characteristic feature is either below the detection limit of our structural data or, more probably, the structure is able to balance low Ba substitution solely by variation of the Me^{2+}/Me^{3+} ratio.

5. Implications

The K-Ba-ferrite from Jabel Harmun, Palestinian Autonomy is the first natural modular ferrite with mixed β″-ferrite (β-alumina) and magnetoplumbite structure. The ideal formula of K-Ba-ferrite can be presented as $K_{0.5}Ba_{0.5}Mg_2Fe_{15.5}O_{26}$ ($Z = 2$) or $KBaMg_4Fe_{31}O_{52}$ ($Z = 1$), and its structure can be described as an alternate stacking of one half β″-ferrite unit cell of $KMg_2Fe_{15}O_{25}$ and one half magnetoplumbite unit cell of $BaMg_2Fe_{16}O_{27}$. This leads to an ordered arrangement of K and Ba in the **c** direction between the *S*-blocks.

The paragenetic association of two stable phases known as synthetic compounds: β″-ferrite ~ $KMg_2Fe_{15}O_{25}$ and *W*-ferrite ~ $BaMg_2Fe_{16}O_{27}$ together with K-Ba-ferrite, which has an ordered mixed structure formed by "supermodules" of the two end-members listed above, represents a highly unusual result. We suggest that K-Ba-ferrite is a transitional alteration product of K-ferrite due to abrupt change in crystallization conditions accompanied by increased Ba activity in the system. The final product of K-ferrite alteration is Ba-ferrite (Fig. 1B). The formation of the ordered "supermodular" structure of K-Ba-ferrite at conditions far from equilibrium suggests that this mixed ferrite may belong to a specific type of dissipative structures (Prigogine & Lefever, 1973) – nano-dissipative structures. It was previously suggested that crystallization of khesinite, both in paralavas and hornfels, resulted from injection of melts/fluids, which reacted with earlier phases, *i.e.*, khesinite and also K- and Ba-ferrites are products of high-temperature alteration of pre-existing pyrometamorphic rocks (Galuskina *et al.*, 2017a).

Acknowledgements: This paper is dedicated to Giovanni Ferraris and Stefano Merlino on the occasion of their 80th birthday. The authors thank two anonymous reviewers for their careful reviews that improved the early version of the manuscript. The work was supported by the National Science Centre (NCN) of Poland, grant no. UMO-2013/11/B/ST10/00272.

References

Bruker (1999): SMART and SAINT-Plus. Versions 6.01. Bruker AXS Inc., Madison, Wisconsin, USA.

Collomb, A., Abdelkader, O., Wolfers, P., Guitel, J.C., Samaras, D. (1986): Crystal structure and magnesium location in the *W*-type hexagonal ferrite: [Ba]Mg_2-W. *J. Magn. Magn. Mater.*, **58**, 247–253.

Galuskin, E., Galuskina, I., Kusz, J., Armbruster, T., Marzec, K., Dzierzanowski, P., Murashko, M. (2014): Vapnikite Ca_3UO_6-a new double perovskite mineral from pyrometamorphic larnite rocks of the Jabel Harmun, Palestine Autonomy, Israel. *Mineral. Mag.*, **78**, 571–581.

Galuskin, E.V., Gfeller, F., Armbruster, T., Galuskina, I.O., Vapnik, Y., Murashko, M., Włodyka, R., Dzierzanowski, P. (2015a): New minerals with a modular structure derived from hatrurite from the pyrometamorphic Hatrurim Complex. part I. Nabimusaite, $KCa_{12}(SiO_4)_4(SO_4)_2O_2F$, from larnite rocks of Jabel Harmun, Palestinian Autonomy, Israel. *Mineral. Mag.*, **79**, 1061–1072.

Galuskin, E.V., Gfeller, F., Armbruster, T., Sharygin, V.V., Galuskina, I.O., Krivovichev, S.V., Vapnik, Y., Murashko, M., Dzierzanowski, P., Wirth, R. (2015b): Mayenite supergroup, part III: fluormayenite, $Ca_{12}Al_{14}O_{32}[\square_4F_2]$, and fluorkyuygenite, $Ca_{12}Al_{14}O_{32}[(H_2O)_4F_2]$, two new minerals from pyrometamorphic rocks of the Hatrurim Complex, South Levant. *Eur. J. Mineral.*, **27**, 123–136.

Galuskina, I.O., Vapnik, Ye., Lazic, B., Armbruster, T., Murashko, M., Galuskin, E.V. (2014): Harmunite $CaFe_2O_4$: a new mineral from the Jabel Harmun, West Bank, Palestinian Autonomy, Israel. *Am. Mineral.*, **99**, 965–975.

Galuskina, I.O., Galuskin, E.V., Pakhomova, A.S., Widmer, R., Armbruster, T., Krüger, B., Grew, E.S., Vapnik, Ye., Dzierazanowski, P., Murashko, M. (2017a): Khesinite, $Ca_4Mg_2Fe_{10}^{3+}O_4[(Si_2)O_{36}]$, a new rhönite-group (sapphirine supergroup) mineral from the Negev Desert, Israel – natural analogue of the SFCA phase. *Eur. J. Mineral*, **29**, 101–116.

Galuskina, I.O., Galuskin, E.V., Prusik, K., Vapnik, Y., Juroszek, R., Jezak, L., Murashko, M. (2017b): Dzierzanowskite, $CaCu_2S_2$–a new natural thiocuprate from Jabel Harmun, Judean Desert, Palestine Autonomy, Israel. *Mineral. Mag.*, **81**, doi:10.1180/minmag.2016.080.153.

Iyi, N. & Göbbels, M. (1996): Crystal structure of the new magnetoplumbite-related compound in the system SrO-Al_2O_3-MgO. *J. Solid State Chem.*, **122**, 46–52.

Juroszek, R., Krüger, H., Galuskina, I.O., Krüger, B., Jezak, L., Ternes, B., Wojdyla, J., Krzykawski, T., Pautov, L.A., Galuskin, E.V. (2017): Sharyginite, IMA 2017-014. CNMNC Newsletter No. 37, June 2017, page 352; *Eur. J. Mineral.*, **29**, 529–533.

Kahn, A. & Thery, J. (1986): Structure of sodium-neodymium aluminate with mixed alumina and magnetoplumbite structure. *J. Solid State Chem.*, **64**, 102–107.

Kolodny, Y. & Gross, S. (1974): Thermal metamorphism by combustion of organic matter: isotopic and petrological evidence. *J. Geol.*, **82**, 489–506.

Kreisel, J., Lucazeau, G., Vincent, H. (1998): Raman spectra and vibrational analysis of $BaFe_{12}O_{19}$ hexagonal ferrite. *J. Solid State Chem.*, **137**, 127–137.

Matsui, Y., Bando, Y., Kitami, Y., Roth, R.S. (1986): High-resolution electron-microscopy study of irradiation induced defects in the β-phase of potassium ferrite. *Acta Crystallogr.*, **B41**, 27–32.

Murashko, M.N., Chukanov, N.V., Mukhanova, A.A. *et al*. (2010): Barioferrite $BaFe_{12}^{3+}O_{19}$ – a new magnetoplumbite-group mineral from Hatrurim Formation, Israel. *Proc. Russ. Miner. Soc.*, **139**, 22–31 [in Russian].

Novikov, I., Vapnik, Ye., Safonova, I. (2013): Mud volcano origin of the Mottled Zone, South Levant. *Geosci. Front.*, **4**, 597–619.

Prigogine, I. & Lefever, R. (1973): Theory of dissipative structures in synergetics. in "Synergetics, Cooperative Phenomena in Multi-Component Systems", H. Haken, ed. Springer Fachmedien Wiesbaden, 124–135.

Pullar, R.C. (2012): Hexagonal ferrites: a review of the synthesis, properties and applications of hexaferrite ceramics. *Progr. Mater. Sci.*, **57**, 1191–1334.

Townes, W.D., Fang, J.H., Perrotta, A.J. (1967): The crystal structure and refinement of ferrimagnetic barium ferrite, $BaFe_{12}O_{19}$. *Z. Kristallogr.*, **125**, 437–449.

Sharygin, V.V., Sokol, E.V., Vapnik, Y. (2008): Minerals of the pseudobinary perovskite-brownmillerite series from combustion metamorphic larnite rocks of the Hatrurim Formation (Israel). *Russ. Geol. Geophys.*, **49**, 709–726.

Sharygin, V.V., Lazic, B., Armbruster, T.M., Murashko, M.N., Wirth, R., Galuskina, I.O., Galuskin, E.V., Vapnik, Y., Britvin, S.N., Logvinova, A.M. (2013): Shulamitite $Ca_3TiFe^{3+}AlO_8$-a new perovskite-related mineral from Hatrurim Basin. *Eur. J. Mineral.*, **25**, 97–111.

Sheldrick, G.M. (1996): SADABS. University of Göttingen, Germany.

— (2008): A short history of SHELX. *Acta Crystallogr.*, **A64**, 112–122.

Silva Júnior, F.M. & Paschoal, C.W.A. (2014): Spin-phonon coupling in $BaFe_{12}O_{19}$ *M*-type hexaferrite. *J. Appl. Phys.*, **116**, 2441–2510.

Received 6 June 2017
Modified version received 27 July 2017
Accepted 31 July 2017